X-Ray Physics: e^+e^- Annihilation

Francisca Vasconcelos*
MIT Department of Physics
(Dated: October 31, 2019)

In this work, we measure the byproducts of e^+e^- annihilation to verify the existence of e^+e^- pairs in an experimental setup consisting of the radioactive isotopes ^{22}Na and ^{60}Co, as well as a High-Purity Germanium (HPGe) detector. In attempts to reduce the systematic errors of our measurements, we further demonstrated the existence of detector artifacts and potential sources of radioactive contamination in the MIT JLAB facility.

I. INTRODUCTION

In 1897, J.J. Thomson discovered the electron (e^-), using cathode ray tubes [1]. Roughly thirty years later, in 1928, Paul Dirac introduced the Dirac Equation. This relativistic wave equation describes all massive spin-$\frac{1}{2}$ particles and postulated the existence of positive-charge electrons [2]. We now know that the positive-charge electron, or positron (e^+), is just one among many types of antimatter particles. However, the positron-electron annihilation process, has many practical applications. Among the most important applications are positron emission tomography (PET) [3], used for nuclear health imaging, and positron annihilation spectroscopy (PAS) [4], used to study voids and defects in solids. In this work, we will measure and analyze the emission spectra of radioactive isotopes, in order to demonstrate the formation and annihilation of e^+e^- pairs.

II. THEORY

II.1. e^+e^- Formation and Annihilation

In the low energy regime ($>$ 1022keV), a photon can interact with an atomic nucleus to undergo pair production. This process generates an e^+e^- pair and residual energy photon,

$$\gamma_\alpha \rightarrow e^- + e^+ + \gamma_\beta, \tag{1}$$

where γ_β has an energy 1022keV less than γ_α. In a normal medium, the positron will quickly encounter a neighboring electron and undergo annhiliation, generating two 511keV gamma rays (γ)

$$e^- + e^+ \rightarrow \gamma + \gamma. \tag{2}$$

This process is illustrated in Fig 1.

II.2. Escape Peaks

Each radioactive source has characteristic peaks in its emission spectra, typically corresponding to gamma ray emission levels in the radionuclei, as demonstrated in Fig 1. If a photon from the source reaches the detector with energy E>1022keV, it can interact with the atoms in the crystal lattice to undergo annihilation. However, the detector will not always pick up all the byproducts of the annihilation. This causes the appearance of what are known as *escape peaks*, within the final measured energy spectra. If an annihilation occurs, there are three different possible measured energy values:

E: The detector picked up on the two 511keV gamma rays, as well as the residual photon. This, however, is indistinguishable from the-no annihilation case.

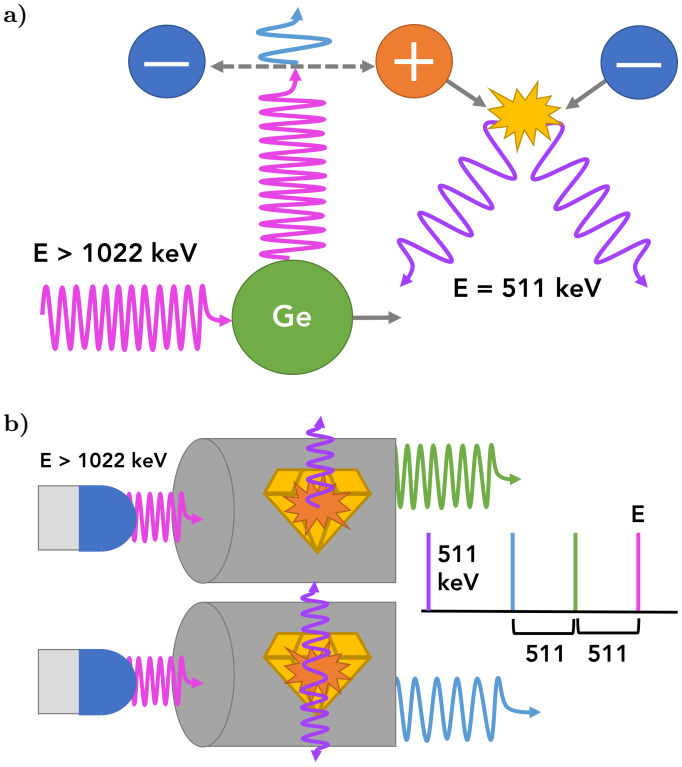

FIG. 1. **(a)** A low energy photon interacts with an atomic nuclei to undergo pair production. An e^+, $e-$, and residual photon are produced. The e^+ annihilates an e^-, generating two 511keV gamma rays. **(b)** Gamma rays produced in annihilation can escape our Germanium crystal detector, resulting in measurements less than the original energy. This causes the appearance of escape peaks in our measured energy spectrum.

* francisc@mit.edu

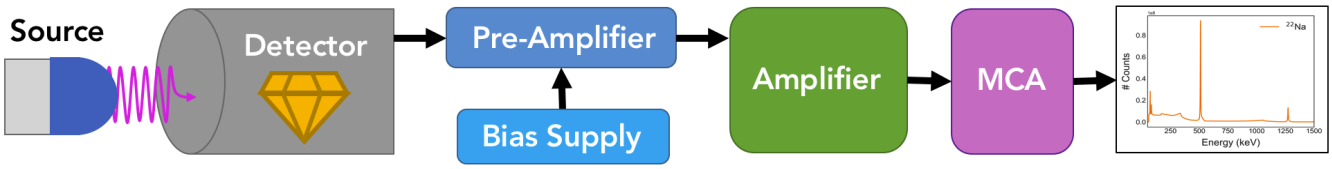

FIG. 2. Here we present a schematic of our measurement chain. Our source radiates photons into an HPGe detector, which converts electron-hole pairs into an electrical signal that is pre-amplified and amplified. Finally, an MCA is used to bin the signal into an energy spectrum histogram.

E-511keV: One of the two 511keV gamma rays "escaped" the detector crystal, without being accounted for in the output electrical signal.

E-1022keV: Both of the 511keV gamma rays "escaped" the detector crystal. Only the residual photon energy was converted into the output electrical signal.

1022keV: The residual energy photon "escaped" the detector crystal. Only gamma ray energy was converted into the output electrical signal.

511keV: The residual energy photon and one of the 511keV gamma rays "escaped" the detector crystal. Only one gamma ray was converted into the output electrical signal.

If the annihilation occurs outside of the detector, i.e. within the plastic cover of the radioactive source, we would expect to see a similar distribution of energy peaks. However, in order to conserve energy/momentum, the two 511keV gamma ray byproducts of e^+e^- annihilation must travel in opposite directions. This means that if annihilation occurs outside of the detector, we would expect to measure at most one of the gamma rays and are limited to the energies: E-511keV, E-1022keV, and 511keV.

III. EXPERIMENTAL SETUP

III.1. Measurement Chain

Our experimental measurement chain is depicted in Fig 2. We placed radioactive sources in front of a High Purity Germanium (HPGe) crystal detector. Using liquid nitrogen, the detector was kept at a temperature near 80K, ensuring a low rate of thermal excitation of electrons into the conduction band of the crystal. Furthermore, in order to sweep out emerging conduction electrons, the crystal was reverse-biased by over +3000 VDC. Photons coming from the radioactive isotope (as well as the background), with energy greater than 1eV, would then create electron-hole pairs within the Ge crystal lattice. Finally, the number of electron-hole pairs (proportional to the energy of radiation interacting with the detector) was converted into an electrical signal.

This signal was then passed through a pre-amplifier, with a positive bias, and amplification unit, with a gain of 88. Positive pulses from the amplification unit were fed into an MCA (multi-channel analyzer), which would record the amplitude of the incoming pulse and bin it into one of 2048 amplitude bins. Each of these bins corresponded to an energy level, but it was necessary to use a calibration source with at least two identifiable peaks of known energy (in our case this was ^{22}Na), so as to assign meaningful energy values to the resulting histogram. This output histogram represents the emission spectrum of the radioactive isotope being measured.

III.2. Radioactive Sources

In our experiment, we performed measurements of three different sources: ^{22}Na, ^{60}Co, and JLAB background radiation. A plot of the resulting measured energy spectra can be found in *AppendixA*. With the goal of demonstrating e^+e^- formation/annihilation, these sources were measured for specific reasons:

^{22}Na: This source is ideal for e^+e^- calibration, since it has a characteristic energy peak at 511keV. This peak, however, is caused by phenomena different from e^+e^- annihilation. It has a secondary, less prominent peak at 1274.5keV which allows us to interpolate the energy axis, when calibrating.

^{60}Co: Since this source has two prominent spectral peaks with energy greater than 1022keV, it is an ideal candidate for measuring e^+e^- formation/annihilation.

JLAB Bkgnd: Measurements of the background noise are critical for performing systematic error analysis.

We began our search for e^+e^- formation/annihilation by looking for a peak at 511keV, created by a gamma ray byproduct, in our measured ^{60}Co spectrum. Initially, we ran a measurement for 1000 seconds, but found that no noticeable peak emerged at 511keV. We unsuccessfully tried mitigating statistical uncertainty by running a longer measurement, of 600,000 seconds. Finally, we moved to a ^{60}Co source that was approximately 100× stronger and ran a 57,370 second measurement. This was successful, and we observed a small peak at 511keV. Analysis of this and other peaks is described in the *Data Analysis* section. A table of the times and number of counts we for each source is included in *Appendix B*.

IV. DATA ANALYSIS

IV.1. Escape Peak Prediction & Detection

Using *Theory* section analysis, we predicted the escape energies of our radioactive isotopes, based on their characteristic energies (>1022keV), as summarized in the "Theory" column of Table I. We found peaks near each of these escape energies in the measured ^{60}Co and ^{22}Na spectra. Since ^{22}Na has a characteristic emission peak at 511keV, we only considered the 511keV peak in the ^{60}Co spectrum for e^+e^- analysis.

We ignored our background measurement for our statistical analysis of these peaks, instead modeling the background as a decaying exponential. We fitted and subtracted this model from both spectra, in order to flatten them for fitting. In order to fit a Gaussian to each peak, we narrowed our scope to a window of roughly 10-30 points surrounding the peak (these were determined by eye, so as to get the best fit). Before performing the fit, the minimum value in the window was determined and subtracted from all points in the window, so as to remove the DC offset. The results and relevant statistics of the Gaussian fit for each peak is summarized in Table I. Additionally, an example fit and data (for the 511keV ^{60}Co peak) is plotted in Fig 3. Plots for the other escape peaks can be found in *Appendix F*.

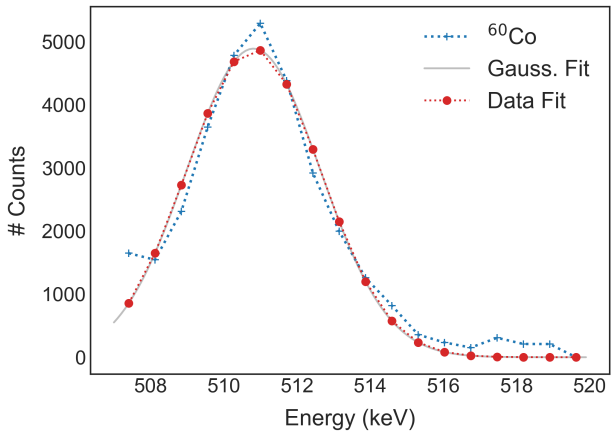

FIG. 3. A Gaussian curve-fit to a peak near our predicted 511keV e^+e^- annihilation energy in ^{60}Co. The # Counts is offset by a modeled background and DC component.

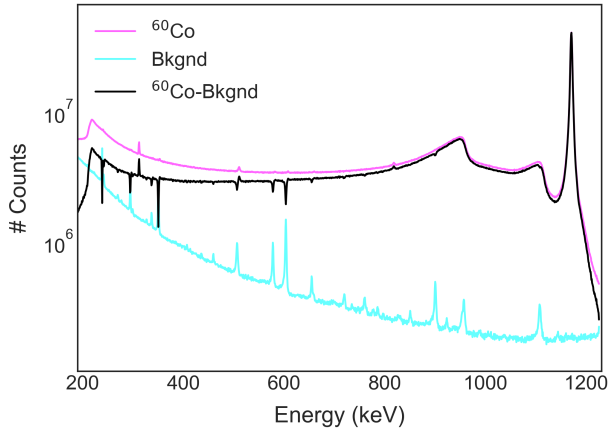

FIG. 4. We subtracted out the background (relatively normalized) from the ^{60}Co spectrum to determine the effect of background radiation on escape peak prominences.

IV.2. Assessing Peak e^+e^- Significance

In order to ensure peaks in our measured spectra were caused by e^+e^- annihilation, we needed to verify that they are more significant than any potential peaks of the same energy in the background radiation spectrum. While in the previous analysis we used an exponential decay model of the background radiation, here we utilized the actual measured background distribution. This spectrum contains several strong peaks, many of which coincide with the predicted escape energies.

In order to compare the ^{22}Na and ^{60}Co spectra with the background spectrum, we needed to normalize all these distributions relative to one another. This was challenging because each source was measured for a significantly different time, with potentially different gain settings in the amplification setup that could affect the count rate (systematic error). Rather than dividing by the total number of counts or multiplying by the time of measurement, we assume that the spectra should have relatively the same composition in the (relatively) low energy regime. We thus selected the energy of 200keV and found the corresponding number of counts in each measurement spectrum at that energy. We calculated the ratio between ^{22}Na and the background, as well as between ^{60}Co and the background at this energy. These ratios were multiplied by the background curve to create normalize it according to the ^{22}Na and ^{60}Co distributions, respectively. Finally, this normalized background curve was subtracted from each distribution, as illustrated with the ^{60}Co curve in Fig 4. We calculated the prominence of the peak in this new spectrum, reported in Table I, to determine if was still prominent (negative prominence means that the background dominated). Note that this peak prominence also accounts for potential calibration error, by reporting the minimum prominence when shifting the background by a few keV (equal to the 2σ uncertainty in the peak).

IV.3. Determining Background Contaminates

We had already postulated the existence of these peaks, at roughly 600keV, because of all the lead bricks and shielding surrounding the detector (lead undergoes Compton scattering at 600keV). However, we were not certain where the remaining peaks came from. Thus, we set out to determine potential sources of radioactive

TABLE I. For each source, the escape peaks of each characteristic energy were computed (Theory). The mean, standard. deviation, amplitude, χ^2 statistics, and prominence (accounting for background radiation) of the Gaussian fit is also reported.

	Theory (Energies)		Gaussian Fit			χ^2-Analysis				Prominence
Source	Characteristic (keV)	Escape (keV)	μ	σ	A	χ^2	df	χ^2_r	Pr(χ^2)	Peak-Bkgd (Counts)
^{60}Co	1173.2	151.2	154.1	0.9	6266	44.9	10	4.5	0	301,312
	1173.2	310.5	312.3	0.7	20810.	133.3	10	13.3	0	-4,401,927
	1173.2, 1332.5	511.0	510.8	1.8	4890.	24.3	17	1.4	0.1115	-369,940
	1332.5	662.2	659.2	1.7	1044	3.41	13	0.3	0.9960	-547,440
	1332.5	821.5	818.2	2.5	3328	33.0	17	1.9	0.0112	162,270
^{22}Na	1274.5	252.5	251.9	0.8	228104	376.0	6	62.7	0	130,000
	1274.5	763.5	762.8	2.18	31218	37.7	12	3.1	0.0001	-373,103

contamination, which could be causing these unexpected peaks. In doing so, we limited our scope of plausible contaminants to the radioactive isotopes used for experiments in Junior Lab. These are described in the experiment descriptions of the JLAB Safety Handout [5]. A copy of the table of isotopes can be found in *Appendix D*.

In order to determine if a listed isotope was a potential contaminant of JLAB, we researched the emission spectrum of each isotope [6]. Each source had at least two characteristic emission energies, usually with one very prominent peak. We looked at those energy levels in our measured background spectrum, to see if there was a corresponding peak, and several were found. In order to deem a particular isotope as a contaminant, we required that there was either a very prominent background peak at the main characteristic energy level or that there were at least two noticeable peaks corresponding to different characteristic energies. Using this approach, we found ^{137}Cs, ^{226}Ra, ^{133}Ba, and ^{109}Cd to be likely contaminants. For a full analysis of these isotopes and their corresponding background peaks, refer to *Appendix E*.

V. RESULTS & CONCLUSIONS

Due to the simple nature of our experimental setup, but goal of measuring the relatively infrequent phenomena of e^+e^- annihilation, the majority of our work focused on mitigating statistical and systematic uncertainties. By simply increasing measurement time and source strength, we were able to see peaks in our data at the predicted escape and e^+e^- annihilation energy levels. The Gaussian fit data in Table I in fact demonstrates that all these peaks fall within roughly 2σ of the predicted escape peak value.

Furthermore, we eliminated the systematic uncertainty of these peaks being caused by background radiation. Although the 511keV peak was not significant due to background radiation, we demonstrated that multiple escape peaks (from the ^{22}Na and ^{60}Co spectra) were still prominent even after subtracting out the measured background. Futhermore, the escape peaks in ^{22}Na were much more prominent and rhobust than those of ^{60}Co, which we believe can be attributed to the longer measurement time of ^{22}Na. Thus, provided more time to measure the ^{60}Co source, we believe we could achieve even more definitive results and potentially have less peaks eliminated by the background. In our efforts to further understand artifacts of our detector, we also performed analysis of *coincidence peaks*, which is described in *Appendix C*.

Finally, in an attempt to understand our systematic uncertainty, we utilized the background measurement to find five potential radiation contaminants in JLAB: ^{82}Pb, ^{137}Cs, ^{226}Ra, ^{133}Ba, and ^{109}Cd. While it has not been proven that these are the only possible sources causing the peaks in the data, we believe that creating a shield to these contaminants around our detector could lead to improved measurement results and eliminate further conflicting sources of error.

In conclusion, we have strong evidence for the existence of e^+e^- formation/annihilation in our setup. In the process of trying to strengthen this claim, we uncovered interesting detector artifacts and potential radioactive contamination in the MIT Junior Lab facility.

ACKNOWLEDGMENTS

FV gratefully acknowledges Ghadah Alshalan's equal partnership, as well as the guidance and advice of the JLAB course staff and faculty.

[1] J. J. T. M. F.R.S., London, Edinburgh, & Dublin Philosophical Magazine & Journal of Science **44**, 293 (1897).
[2] P. A. M. Dirac, *The Principles of Quantum Mechanics* (Clarendon Press, 1930).
[3] D. L. Bailey, M. N. Maisey, D. W. Townsend, and P. E. Valk, *Positron emission tomography* (Springer, 2005).
[4] R. Siegel, Annual Review of Materials Science **10**, 393 (1980).
[5] *JLAB Safety Handount* (MIT Physics Department).
[6] *Live Chart of Nuclides* (IAEA Nuclear Data Section).

Appendix A: Radiation Spectra

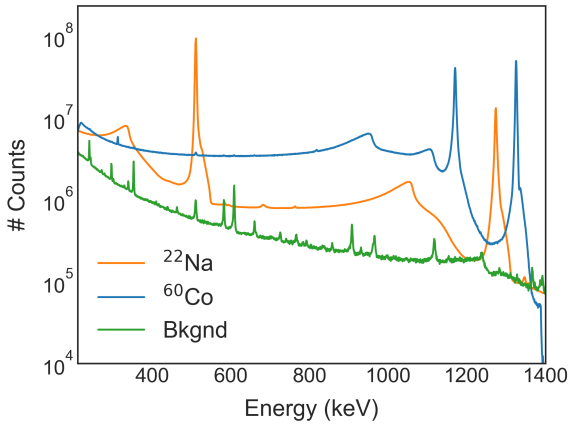

FIG. 5. A figure of the long measured spectra of ^{22}Na, ^{60}Co, and the JLAB Background. These were normalized as described in the *Assessing Peak e^+e^- Significance* section.

Appendix B: Measurement Times and Counts

TABLE II. The data collection time, total number of counts, and ratio of these two quantities (count rate).

Source	Time (s)	# Counts	Count Rate ($\frac{counts}{sec}$)
^{22}Na	315,583	3,326,539,097	10,541
^{60}Co	57,370	121,839,100	2,124
Bkgnd	229,235	15,658,002	68

Appendix C: Coincidence Peaks

1. Theory

In the case of escape peaks, we discussed a detector artifact in which the reported energy is less than the actual energy emitted by our radioactive source. However, in the case of another artifact, known as *coincidence peaks*, we expect to see an opposite effect.

Given a radioactive source with prominent spectral peaks at energies E_α and E_β, we generally would expect to measure either E_α or E_β. However, a very small number of times, we can imagine that two emitted photons would hit the detector at essentially the same time. In this case, the detector would report the sum of energies. Thus, for the source described, we would expect to see additional peaks at E_α+E_β,2E_α, and E_β. These are called the coincidence peaks and, as demonstrated in the *Analysis* portion of this paper, we can calculate the likelihood of each of the coincidences, provided measurements.

2. Peak Prediction and Detection

Since ^{22}Na has peaks at 511keV and 1274keV, we would expect that very infrequently an emission at both of these energies would hit the detector at the same time, resulting in a measurement of 1785 keV. Given that we took over 3 billion measurements, we would expect to see a small peak at this energy in our spectrum. By plotting on a logarithmic scale, we already see the emergence of a prominent third peak. Similarly to our analysis of the escape peaks, we subtracted a modeled exponential background noise and performed a Gaussian curve fit. However, as shown in Fig 2, the data was not well represented by a Gaussian, but actually extremely Lorentzian in its form. After fitting to a Cauchy distribution,

$$f(x;x_0,\gamma) = \frac{1}{\pi\gamma}\left[\frac{\gamma^2}{(x-x_0)^2+\gamma^2}\right] \tag{C1}$$

we found $x_0 = 1789$ (location of maxima) and $\gamma = 6.75$ ($\frac{1}{2}$FWHM).

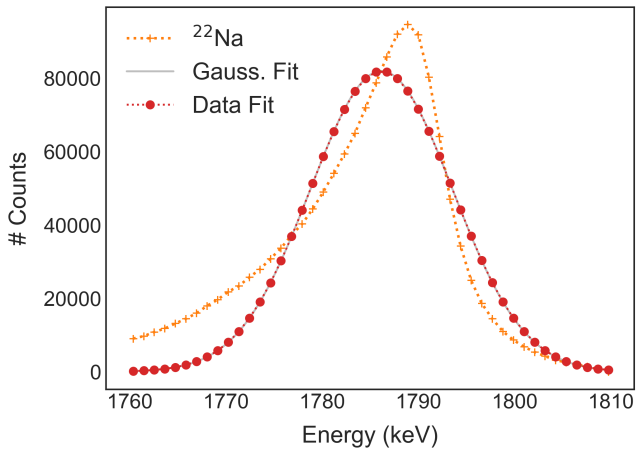

3. Likelihood of Coincidence

Finally, we calculated the likelihood of such a coincidence happening in our detector. This was done by first calculating the prominence of the 511keV (9.2×10^7 counts), 1274keV (1.3×10^7 counts), and 1785keV (or as we found 1789keV) peak (9.5×10^4 counts). In order to calculate the relative ratios of observing either or both of these counts, we divide the prominence of that specific peak by the sum of all prominence. Thus, we calculate the following probabilites:

$$\Pr(511\text{keV}) = \frac{9.2\times10^7}{1.05095\times10^8} = 87.53984\% \tag{C2}$$

$$\Pr(1274\text{keV}) = \frac{1.3 \times 10^7}{1.05095 \times 10^8} = 12.369976\% \quad \text{(C3)}$$

$$\Pr(1785\text{keV}) = \frac{9.5 \times 10^4}{1.05095 \times 10^8} = 0.09039\% \quad \text{(C4)}$$

As we expected, the likelihood of measuring such a coincidence is essentially negligible. However, it is quite a feat that we were able to detect such a peak, based on the sheer number of measurements we performed. Furthermore, we can be certain that this peak came purely from coincidences because at high energies (including the 1700s range we were measuring in), the gamma rays become so energetic that they pass straight through our HPGe detector without being detected.

Appendix D: JLAB Experiment Isotopes

TABLE I. A table showing the radioactive sources used in Junior Lab and their approximate activities.

Experiment	Isotope	~ Activity (mCi)
Compton Scattering	^{137}Cs	0.4
Mössbauer Spectroscopy	^{57}Co	4
Rutherford Scattering	^{241}Am	0.2
Alpha Decay	Uranium Ore	5×10^{-6}
	^{226}Rd	0.013
Relativistic Dynamics	^{90}Sr	8
	^{133}Ba	0.08
X-Ray Physics	^{241}Am	10
	^{55}Fe	0.7
	^{90}Sr	0.6
	^{57}Co	0.02
Calibration Sources	^{133}Ba	0.005
	^{109}Cd	0.008
	^{137}Cs	0.007
	^{57}Co	0.0001
	^{60}Co	0.01
	^{54}Mn	0.0002
	^{22}Na	0.01

Source: JLAB Safety Handout [5]

Appendix E: Background Contamination Peak Analysis

We presented logic as to why we believe lead is a contaminant in the paper. To demonstrate why we believe the sources ^{137}Cs, ^{226}Ra, ^{133}Ba, and ^{109}Cd are also contaminants, we present a table in which we list the most prominent characteristic energy peaks of each source. Energies listed in the "Strong Peaks" column correspond to the most prominent peaks in the emission spectra of the source. Energies listed in the "Weak Peaks" column correspond to noticeable peaks in the spectrum that are not as prominent. Energy levels colored in green correspond to energy levels in the measured background that had significant peaks, while red boxes correspond to those that did not. Energy levels that fell outside of our measured spectrum are colored in yellow.

Source	Strong Peaks (keV)			Weak Peaks (keV)			
^{137}Cs	30	662					
^{57}Co	14	122		136			
^{241}Am	60			14	18	20	26
Uranium	98			105	185		
^{226}Ra	186						
^{90}Sr	546	228					
^{133}Ba	31	81	356	276	302	383	
^{35}Fe	6						
^{109}Cd	22			88			
^{54}Mn	821			239			
^{22}Na	511			1274			
^{60}Co	1173	1332					

Despite the criterion we set in the paper for determining if a source was a contaminant, we refrained from calling ^{22}Na a contaminant because we know that the 511keV peak can be attributed to e^+e^- annihilation created by any radioactive source with energy higher than 1022keV.

Appendix F: Escape Peak Fitting and Plots

In the paper, we included the data and Gaussian fit for our 511keV ^{60}Co source. We now present the remaining data and curve fit for the four ^{60}Co escape peaks and the two ^{22}Na, ordered in terms of increasing energy.

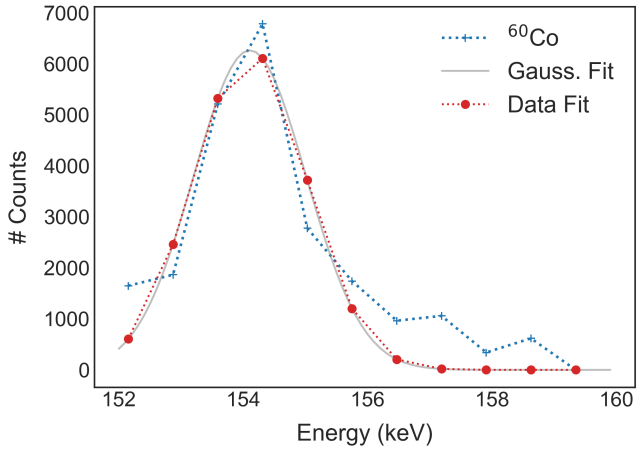

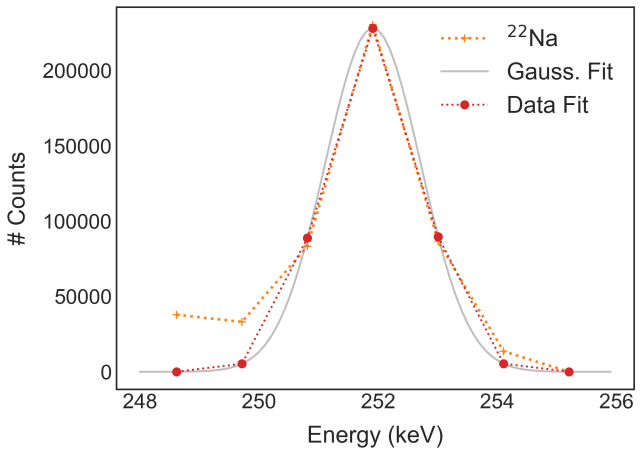
^{22}Na
Gauss. Fit
Data Fit
Counts
Energy (keV)
0
50000
100000
150000
200000
248
250
252
254
256

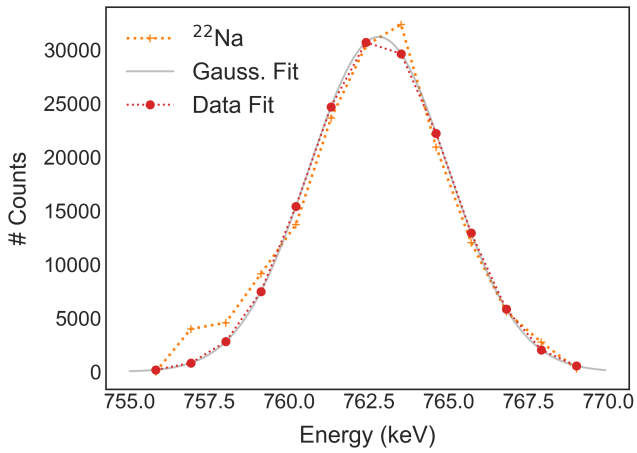
^{22}Na
Gauss. Fit
Data Fit
Counts
Energy (keV)
0
5000
10000
15000
20000
25000
30000
755.0
757.5
760.0
762.5
765.0
767.5
770.0

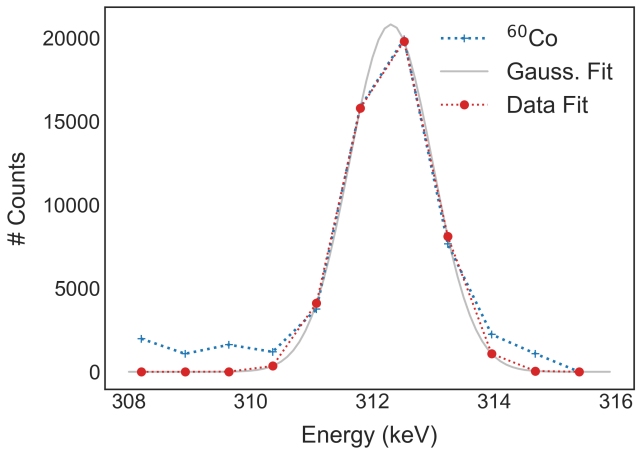
^{60}Co
Gauss. Fit
Data Fit
Counts
Energy (keV)
0
5000
10000
15000
20000
308
310
312
314
316

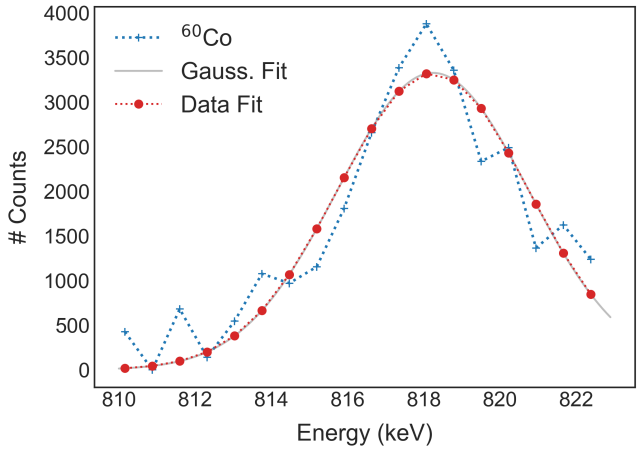
^{60}Co
Gauss. Fit
Data Fit
Counts
Energy (keV)
0
500
1000
1500
2000
2500
3000
3500
4000
810
812
814
816
818
820
822

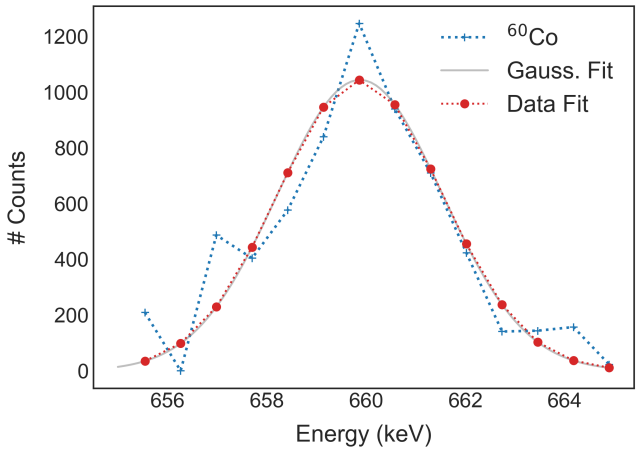
^{60}Co
Gauss. Fit
Data Fit
Counts
Energy (keV)
0
200
400
600
800
1000
1200
656
658
660
662
664